Numerical Solution of the Navier-Stokes Equation for Flow Past Spheres: Part I. Viscous Flow Around Spheres with and Without Radial Mass Efflux

A. E. HAMIELEC, T. W. HOFFMAN
McMaster University, Hamilton, Ontario, Canada

L. L. ROSS
Chemical Projects, Ltd., Toronto, Ontario, Canada

This study was undertaken to ascertain the accuracy of finite-difference solutions for flow around spherical particles in the intermediate Reynolds number range. Comparison of the results with experimental data on drag coefficients, frontal stagnation pressure, and wake geometry indicated good agreement. The approximate solutions, in which the Galerkin method and asymptotic analytical predictions were utilized, were evaluated by using the finite-difference solutions as a standard. These methods were used to calculate the effect of uniform and nonuniform mass efflux on the drag and flow characteristics around a sphere. Theoretical solutions indicated that nonuniform mass efflux can significantly reduce the drag on a submerged object. Ranges of applicability of the approximate methods were established.

The laws of motion of a single spherical partical in an undisturbed fluid stream (that is, one in which there is no secondary motion) have been the subject of many investigations (*1, 2*). The macroscopic hydrodynamical characteristics, exemplified by the drag coefficient, are well-established over a large Reynolds number range by numerous experimental studies (3 to 7). Obtained from these data are a number of quite accurate experimental correlations (*8* to *10*) over the range of interest in the present study ($0 \lesssim N_{Re} \lesssim 500$). More detailed investigations (*11* to *14*) reveal not only widely differing flow patterns in the various Reynolds number regimes, but also indicate that the region of present interest is very little understood. This lack of knowledge is best exemplified by conflicting evidence of the first appearance of a vortex ring (*15* to *17*). We believe that the most reliable experimental investigation of the wake region is that of Taneda (*17*).

An analytical solution of the complete Navier-Stokes equations is impossible at the present time owing to their nonlinearity. Although numerous approximate solutions have been obtained (*18* to *21*, *22* to *39*), virtually the only exact solutions available are those of Stokes (*40*) (that is, $N_{Re} \lesssim 1$) and the potential flow solution. The most successful approximate solutions have been obtained by use of the boundary-layer assumptions (*22* to *32*). Although the literature contains an almost endless number of techniques for solving the boundary-layer equations, the most rigorous and accurate solution is that of Frossling (*32*). For the frontal stagnation point the theoretical treatment of Homann (*42*) probably yields the most accurate results.

Although the lower Reynolds number limit of applicability of the boundary-layer solutions should be well above 200, they have been widely applied well below this value. Experimental justification of this extrapolation, for example, by the comparison of theoretical and experimental drag coefficients, has not been possible as the boundary-layer solutions are only applicable up to the flow separation point. At present there is no adequate mathematical description of the wake region. Thus, the boundary-layer solutions, although yielding accurate results up to the flow separation point, cannot be used to describe the entire flow field.

A number of approximate descriptions of the entire flow field through the use of trial stream function polynomials with subsequent determination of the constants in the polynomials using variational or error-distribution methods have been presented (*39, 41, 33* to *36*). In particular, Kawaguti used the Galerkin method with two trial stream functions to investigate the region, $N_{Re} \lesssim 20$ and $20 \lesssim N_{Re} \lesssim 70$. Recently these solutions were extended to include the entire laminar flow regime (*34, 35*).†

The use of finite-difference methods has met with moderate success in yielding an overall description of the flow field (*38*). Unfortunately, solutions for $N_{Re} > 40$ are not available.

At present virtually no theoretical treatments of the interaction of a normal interfacial velocity on the forced-convection flow field around a sphere in the regime of present interest exist. Theoretical work has been restricted to boundary-layer solutions (*23* to *25*) that use invalid interfacial velocities.

The present study was undertaken to ascertain the ability of a finite-difference method to predict flow behavior around spherical particles in the intermediate Reynolds number range. Once the accuracy of the finite-difference solutions was established, approximate solutions, such as those obtained from application of the Galerkin method or the linearized Navier-Stokes equations, could then be evaluated for a number of specific problems. Moreover, the problems under study were chosen for their practical interest so that a number of conclusions could be made concerning the particular phenomenon.

† These investigators and also Flumerfelt and Slattery (*36*) have noted an error in Kawaguti's original work.

THEORY

The Navier-Stokes equation for viscous, incompressible, axisymmetric flow in terms of the stream function Ψ in spherical coordinates may be written as

$$\frac{N_{Re}}{2}\left[\frac{\partial\Psi}{\partial r}\cdot\frac{\partial}{\partial\theta}\left(\frac{E^2\Psi}{r^2\sin^2\theta}\right)-\frac{\partial\Psi}{\partial\theta}\cdot\frac{\partial}{\partial r}\left(\frac{E^2\Psi}{r^2\sin^2\theta}\right)\right]\sin\theta=E^4\Psi \quad (1)$$

where

$$E^2=\frac{\partial^2}{\partial r^2}+\frac{\sin\theta}{r^2}\frac{\partial}{\partial\theta}\left(\frac{1}{\sin\theta}\frac{\partial}{\partial\theta}\right)$$

Equation (1) may be split into two simultaneous second-order equations by introducing the vorticity ζ as follows:

$$E^2\Psi=\zeta r\sin\theta \quad (2)$$

$$\frac{N_{Re}}{2}\left[\frac{\partial\Psi}{\partial r}\cdot\frac{\partial}{\partial\theta}\left(\frac{\zeta}{r\sin\theta}\right)-\frac{\partial\Psi}{\partial\theta}\cdot\frac{\partial}{\partial r}\left(\frac{\zeta}{r\sin\theta}\right)\right]\sin\theta=E^2(\zeta r\sin\theta) \quad (3)$$

The velocity components are related to the stream function as follows:

$$V_\theta=\frac{1}{r\sin\theta}\frac{\partial\Psi}{\partial r};\quad V_r=\frac{-1}{r^2\sin\theta}\frac{\partial\Psi}{\partial\theta}$$

All quantities have been made dimensionless by putting

$$r=\frac{r'}{A},\quad \Psi=\frac{\Psi'}{UA^2},\quad \zeta=\frac{\zeta' A}{U},\quad V_r=\frac{V'_r}{U},$$

$$V_\theta=\frac{V'_\theta}{U},\quad N_{Re}=\frac{2UA}{\nu}$$

Three methods to solve Equations (1), (2), and (3) have been attempted and these will be discussed in turn. The application of these methods of solution to various problems (various boundary conditions) will then follow.

METHODS OF SOLUTION

Analytical Method

In the limit as $N_{Re}\longrightarrow 0$, Equation (1) reduces to the linear asymptotic form

$$E^4\Psi=0 \quad (4)$$

The Stokes solution may be expressed as

$$\Psi=(A/r+Br+Cr^2+Dr^4)\sin^2\theta \quad (4a)$$

This equation has a range of applicability that depends upon the boundary conditions employed. For rigid spheres ($V_r=V_\theta=0$ at $r=1$) in an infinite fluid, the accuracy is considered adequate for most applications at Reynolds number less than 0.1.

Oseen (*18*) assumed that the sphere caused a small perturbation to parallel flow and neglected second-order perturbation velocities, taking the quadratic inertia terms partly into account. This method gives solutions that are considered inadequate above a Reynolds number of 2. At higher Reynolds numbers there are no available analytical solutions to Equations (1) or (2) and (3).

Finite-Difference Method

The most recent investigation concerned with solving Equations (2) and (3) with a finite-difference method was by Jenson (*38*). Relaxation techniques and a desk calculator were employed to obtain solutions for rigid spheres at Reynolds numbers of 5, 10, 20, and 40. Finite-difference equations [Equations (7) and (8)] were derived by using a Taylor series expansion correct to the second order. Finite-difference equations correct to the second and fourth order gave similar results for the particular case of $N_{Re}=5$. This suggested that equations correct to second order adequately represent the equations of motion. Jenson's choice of angular step size (6 deg.) is too large to give results that enable the wake characteristics to be thoroughly investigated.

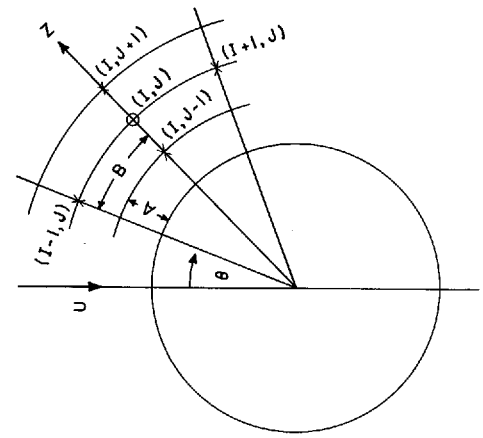

Fig. 1. Circular mesh system.

The present investigation is aimed at extending Jenson's work to higher Reynolds numbers with the aid of a digital computer. The finite-difference equations accurate to second order derived by Jenson have been used throughout this investigation, as well as an exponential step size in the radial direction and a constant angular step size. The stream function and vorticity vary most rapidly near the sphere, thus requiring a small step size there. A larger step size far from the surface is adequate. This is achieved by using equal intervals in Z, ($r=e^Z$); namely Equations (2) and (3) become

$$e^{2Z}E^2\Psi-\zeta e^{3Z}\sin\theta=0 \quad (5)$$

$$\frac{N_{Re}}{2}\left[\frac{\partial\Psi}{\partial Z}\cdot\frac{\partial F}{\partial\theta}-\frac{\partial\Psi}{\partial\theta}\frac{\partial F}{\partial Z}\right]e^Z\sin\theta-e^{2Z}E^2G=0 \quad (6)$$

where

$$e^{2Z}E^2=\frac{\partial^2}{\partial Z^2}-\frac{\partial}{\partial Z}+\sin\theta\frac{\partial}{\partial\theta}\left(\frac{1}{\sin\theta}\frac{\partial}{\partial\theta}\right)$$

$$F=\frac{\zeta}{e^Z\sin\theta},\quad G=\zeta e^Z\sin\theta$$

The circular mesh system employed is shown in Figure 1.

By considering lattice spacing A in the Z direction and B in the θ direction, Equations (5) and (6) may be written in finite-difference form as

$$\Psi(I,J+1)\left(\frac{2-A}{2A^2}\right)+\Psi(I,J-1)\left(\frac{2+A}{2A^2}\right)+\Psi(I+1,J)\left(\frac{2-B\cot\theta(I)}{2B^2}\right)+\Psi(I-1,J)\left(\frac{2+B\cot\theta(I)}{2B^2}\right)-\Psi(I,J)\left(\frac{2}{A^2}+\frac{2}{B^2}\right)-G(I,J)e^{2Z(J)}=0 \quad (7)$$

$$G(I,J+1)\left(\frac{2-A}{2A^2}\right)+G(I,J-1)\left(\frac{2+A}{2A^2}\right)$$
$$+G(I+1,J)\left(\frac{2-B\cot\theta(I)}{2B^2}\right)$$
$$+G(I-1,J)\left(\frac{2+B\cot\theta(I)}{2B^2}\right)$$
$$-G(I,J)\left(\frac{2}{A^2}+\frac{2}{B^2}\right)-\frac{N_{Re}}{4}e^{Z(J)}\sin\theta(I)$$
$$\left[\left(\frac{\Psi(I,J+1)-\Psi(I,J-1)}{2A}\right)\left(\frac{F(I+1,J)-F(I-1,J)}{B}\right)-\left(\frac{\Psi(I+1,J)-\Psi(I-1,J)}{2B}\right)\left(\frac{F(I,J+1)-F(I,J-1)}{A}\right)\right]=0 \quad (8)$$

In the iterative procedure used to solve Equations (7) and (8) relaxation factors were used to stabilize the computations. They were introduced as follows:

$$\Psi_n(I,J)=\Psi_{n-1}(I,J)+WW\,[\Psi_n^*(I,J)-\Psi_{n-1}(I,J)] \quad (9)$$

$$G_n(I,J)=G_{n-1}(I,J)+W\,[G_n^*(I,J)-G_{n-1}(I,J)] \quad (10)$$

where subscript n denotes the n^{th} value calculated and the asterisk denotes the value calculated by using Equations (7) and (8).

A criterion proposed by Jenson (38) was used as a guide in initially choosing a step size for the computation, and is discussed in detail in Part II of this paper. Starting values for Ψ and G were obtained by using polynomial expressions derived approximately with an error-distribution method. This approximate method is discussed in this paper.

Error-Distribution Method (Galerkin Method)

In a recent paper Snyder, Spriggs, and Stewart (41) made a survey of the application of Galerkin's method to the solution of problems in fluid mechanics. Essentially the method involves choosing a trial polynomial that is made to satisfy all boundary conditions and the differential equation approximately by using orthogonality principles. The success of this method depends strongly on the choice of the trial polynomial.

APPLICATION TO PARTICULAR PROBLEMS

Zero Radial Mass Efflux

Boundary Conditions. When solving Equation (1) or (4) the stream function and its derivatives must be specified on a boundary that completely encloses the region of flow. The boundary conditions are

Along the axis of symmetry

$$\theta=0^\circ \text{ and } \theta=180^\circ,\ \Psi=0 \quad (11)$$

On the sphere surface

$$r=1\ \ \Psi=0 \text{ and } \frac{\partial\Psi}{\partial r}=0 \quad (12)$$

Far from the sphere there is undisturbed parallel flow

$$r=\infty\ \ \Psi=\frac{1}{2}r^2\sin^2\theta \quad (13)$$

Moreover, when solving Equations (2) and (3) or (5) and (6) boundary conditions are required that specify Ψ and ζ.

Along the axis of symmetry

$$\theta=0^\circ \text{ and } \theta=180^\circ\ \Psi=0,\ \zeta=0 \quad (11a)$$

On the sphere surface

$$r=1\ \ \Psi=0,\ \ \zeta=\frac{E^2\Psi}{\sin\theta} \quad (12a)$$

Far from the sphere there is undisturbed parallel flow

$$r=\infty\ \Psi=\frac{1}{2}r^2\sin^2\theta,\ \zeta=0 \quad (13a)$$

When considering a finite boundary, the disturbance to parallel flow caused by the sphere is set equal to zero on a concentric spherical boundary moving with the sphere, that is Equation (13*a*) is applied at $r=R$.

METHODS OF SOLUTION

Analytical Method

The solution of Equation (4) after Stokes is

$$\Psi=(A/r+Br+Cr^2+Dr^4)\sin^2\theta \quad (14)$$

For the case of an infinite fluid this becomes

$$\Psi=\left(\frac{1}{2}r^2+\frac{1}{4r}-\frac{3}{4}r\right)\sin^2\theta \quad (14a)$$

The constants in Equation (14) can also be found by satisfying the following boundary conditions:

$$r=1 \qquad \Psi=0, \qquad \frac{\partial\Psi}{\partial r}=0$$
$$r=R \qquad \Psi=\frac{1}{2}R^2\sin^2\theta,\ \zeta=0 \quad (14b)$$

These boundary conditions are identical to those satisfied in the finite-difference method used in this study. The constants are related to R as follows:

$$B=\frac{15/2R^6}{(2-10R^3+18R^5-10R^6)} \quad (15a)$$

$$C=\frac{-5/2R^3-5R^6}{(2-10R^3+18R^5-10R^6)} \quad (15b)$$

$$D=\frac{3/2R^3}{(2-10R^3+18R^5-10R^6)} \quad (15c)$$

The total drag coefficient is given by

$$C_D=\frac{-32B}{N_{Re}} \quad (15d)$$

Finite-Difference Method

Boundary condition (12*a*) takes the following finite-difference form:

$$\zeta(I,1)=\frac{8\Psi(I,2)-\Psi(I,3)-7\Psi(I,1)}{2A^2\sin\theta(I)} \quad (16)$$

In the derivation of this equation, the derivative $\partial\Psi/\partial r$ is set equal to zero, thus satisfying the condition that $(V_\theta)_{r=1}=0$.

Radial and angular step sizes were varied to test the accuracy of these solutions. The position of the outer spherical boundary was changed to investigate the effect of wall proximity. The choice of relaxation factors was simply by trial and error. These factors were lowered in magnitude until the oscillation of vorticity near the outer

boundary was reduced or eliminated, giving stable solutions.

Finite-difference solutions were obtained by using IBM 7040 and 7094 computers.

Error-Distribution Method (Galerkin Method)

Kawaguti (39) used a special series of Legendre polynomials as a trial stream function and used the Galerkin method to satisfy the Navier-Stokes equations. In the original paper by Kawaguti solutions were obtained for an infinite fluid for Reynolds numbers up to 70. Hamielec et al. (35), using the identical method, carried the computations to Reynolds numbers above 500. The success of this method depends greatly upon the choice of trial stream function, and hence cannot be expected to apply adequately over a large Reynolds number range.

The trial stream function used by Kawaguti and later by Hamielec et al. was of the form

$$\Psi = \left(\frac{1}{2}r^2 + \frac{A_1}{r} + \frac{A_2}{r^2} + \frac{A_3}{r^3} + \frac{A_4}{r^4}\right)\sin^2\theta + \left(\frac{B_1}{r} + \frac{B_2}{r^2} + \frac{B_3}{r^3} + \frac{B_4}{r^4}\right)\sin^2\theta\cos\theta \quad (17)$$

The constants $A_1, \ldots, A_4$, and $B_1, \ldots, B_4$ were determined by satisfying boundary conditions and the Navier-Stokes equations by using orthogonality principles. These constants have been tabulated (35) for the entire laminar flow regime. The accuracy of these solutions has so far not been investigated in detail.

DISCUSSION OF RESULTS

Solutions were obtained by using IBM 7040 and 7094 digital computers. The effect of radial and angular step size on the accuracy of the finite-difference solutions for $N_{Re} \leq 40$ was investigated in detail and shown to be negligible for the step sizes used. Computation time limitations made investigation of the effect of step size at higher Reynolds numbers impractical. However for the solutions at $N_{Re} = 100$, a radial step size of $A = 0.025$ and an angular step size of 3 deg. were assumed to be sufficiently small to give adequate accuracy. To test the accuracy by other means, predicted results were compared with some reported experimental observations of flow behavior around rigid spheres, drag coefficients, and frontal stagnation pressures as a function of Reynolds number. For example, Figure 2 illustrates the excellent agreement of the predicted wake dimensions with those measured by Taneda (17). This agreement is remarkable in view of the complex flow in the vortex region. A critical Reynolds

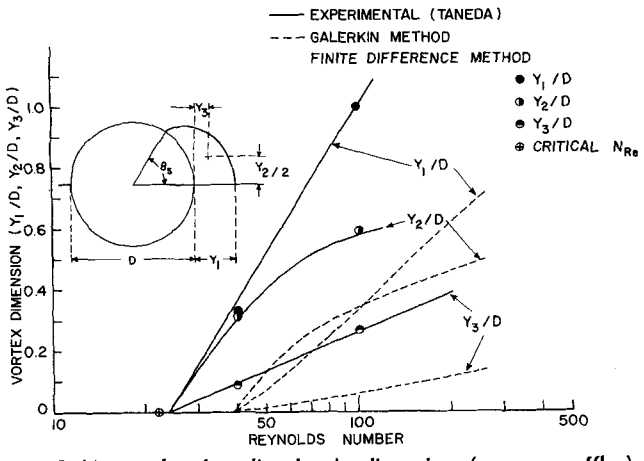

Fig. 2. Measured and predicted wake dimensions (zero mass efflux).

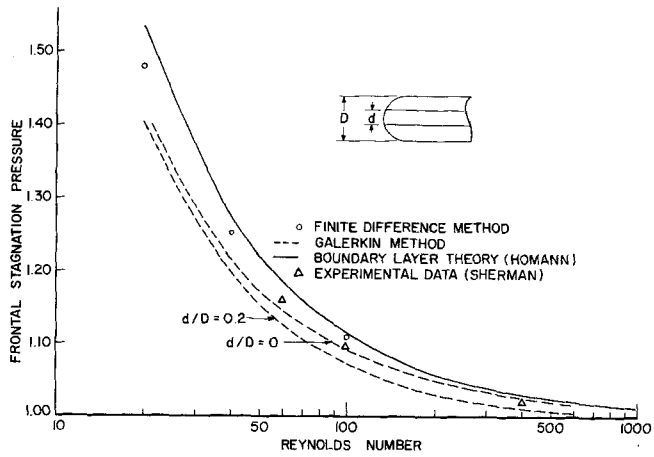

Fig. 3. Measured and predicted frontal stagnation pressures (zero mass efflux).

number for flow separation of 22 was estimated. Jenson (38) found a value of 17. Disagreement is to be expected because of the limitations due to a finite step size. Jenson used an angular step size of 12 deg.; we a 3-deg. step size. If the angle of flow separation were less than 3 deg., presumably the presence of a vortex ring would not be detected. Moreover, with reference to Figure 3, the agreement of the predicted frontal stagnation pressure with the analysis of Homann (42) and the experimental observations of Sherman (44), which were made with a spherical nose Pitot tube, lends additional support to the adequacy of the method to predict local behavior. The slight differences can be attributed to the finite dimensions of the pressure tap, which necessarily implies integration, and the fact that slip may occur over this area. Of course, these effects may be taken into account if a more rigorous analysis is warranted.

Table 1 shows a comparison of experimental and calculated drag coefficients for various Reynolds numbers. Predictions to within 8% are possible and this accuracy can be seen to be affected by the position of the finite spherical boundary. Unfortunately, computation time was found to increase significantly as the boundary was moved away from the sphere and this increase was further magnified as the Reynolds numbers were increased. This result arises because we believed that at higher Reynolds numbers, a small radial step size (for example $A = 0.025$) was necessary and that prediction of the details of the flow field required an angular step size no greater than 3 deg. Therefore, the outer boundary must be kept to a minimum to ensure reasonable computational times. Fortunately, local values of vorticity and pressure were not significantly

Table 1. Comparison of Finite-Difference Results with Experimental Drag Coefficients (Zero radial mass flux)

N_{Re}	R	C_D (finite difference)	C_D (experimental) (for an infinite fluid)*
0.1	19.1	262	240
1.0	47	27.5	26.5
1.0	7.0	32.5	26.5
20	12.2	2.78	2.55
20	7.0	2.88	2.55
40	14.6	1.86	1.70
40	7.0	1.89	1.70
100	7.0	1.12	1.07

* Lapple (7).

Table 2. Comparison of Finite-Difference Results with Drag Coefficients Found by Using Analytical Methods (Zero radial mass flux)

$N_{Re} = 0.1$

R	C_D (finite difference)	C_D (analytical*)	C_D (analytical†)
2.01	1,059	1,082	1,949
3.86	433	438	522
7.05	320	319	349
12.25	279	281	294
19.14	262	265	272
∞	—	240	240

* Equation (14).
† Satapathy and Smith (43).

affected by movement of the boundary through the limits indicated in Table 1. However, the resulting small errors are magnified when these variables are integrated to yield drag coefficients and the results presented in Table 1 bear this out.

It was found that the outer boundary for undisturbed flow must be at a relatively large radial distance for low Reynolds numbers. This wall effect was investigated in detail at a Reynolds number of 0.1 and is compared with the predictions of Satapathy and Smith (43) and with the present analytical solution in Table 2. The agreement with Equation (14), subject to the boundary conditions given by Equation (14*b*), suggests that the accuracy of the finite-difference method is satisfactory and that deviations from experimental data for an infinite fluid are due principally to wall effects and not to errors inherent in the finite-difference approach to the solution.

With this established confidence in the finite-difference method, the ability of the approximate Galerkin method to predict flow behavior, vorticity, and pressure distribution may be evaluated. Figures 2 to 6 show this comparison. Referring to Figure 2 it is obvious that the dimensions of the vortex ring predicted by the Galerkin method are highly inaccurate. It is of interest to note however that the predicted change in vortex shape with Reynolds number is quite similar to that measured by Taneda (17). The critical Reynolds number of 39 is of course much too large. A comparison of stagnation streamlines in Figure 4 again emphasizes the inability of the Galerkin method to predict accurately flow behavior in the vortex region. It might be pointed out that a more severe test would have been the comparison of predicted lines of constant vorticity as these vary substantially with change in Reynolds number. However, the disagreement was quite obvious even though streamlines were compared. Indeed, the streamlines describing the wake flow at $N_{Re} = 500$ are certainly not realistic. It is well known that vortex shedding occurs at $N_{Re} \sim 400$ and even if shedding were prevented the true vortex ring would have a much more streamlined shape.

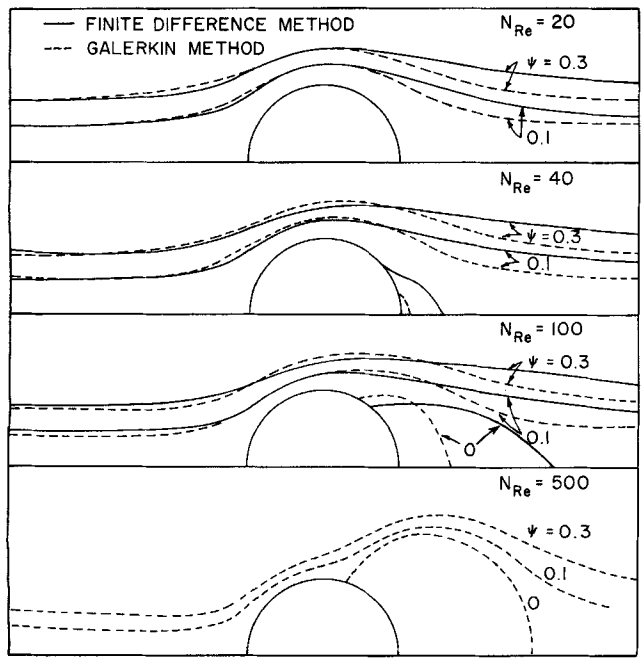

Fig. 4. Streamlines predicted by Galerkin and finite-difference methods (zero mass efflux).

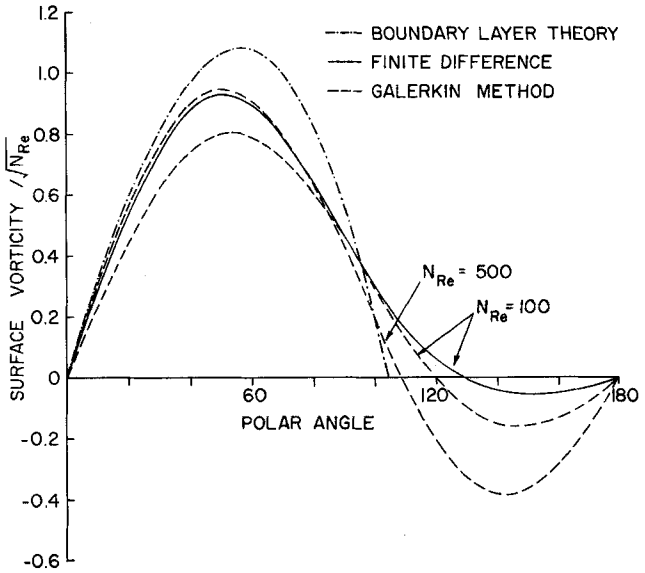

Fig. 5. Surface vorticity distributions predicted by Galerkin and finite-difference methods compared with boundary-layer theory (zero mass efflux).

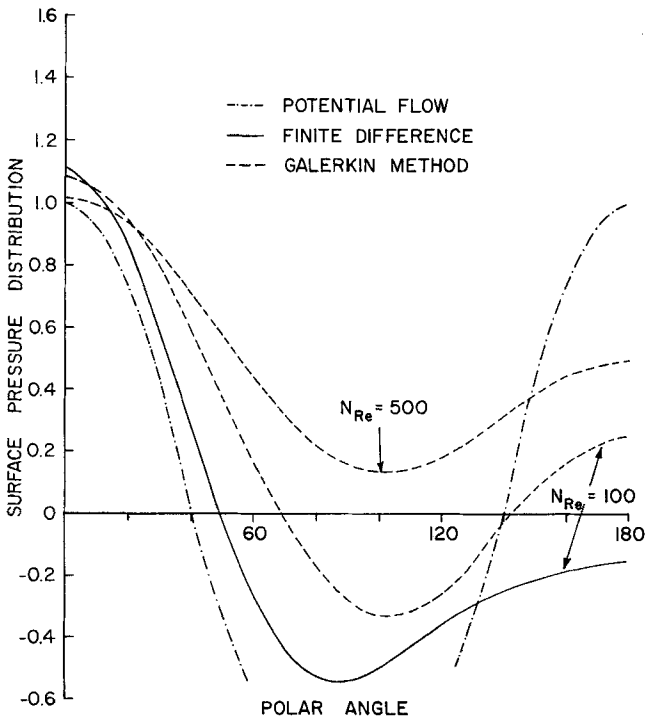

Fig. 6. Surface pressure distributions predicted by Galerkin and finite-difference methods compared with potential flow theory (zero mass efflux).

Correct trends in surface vorticity are predicted but the results are somewhat low at any given Reynolds number (see Figure 5). A comparison of the finite-difference result with boundary-layer theory indicates that the latter yields fairly accurate surface vorticities up to the separation point even for Reynolds numbers as low as 100. This suggests that predictions of local Nusselt numbers for forced convection transfer by using the surface vorticity distribution obtained from boundary-layer theory should be fairly accurate at these low Reynolds numbers. The momentum boundary layer would of course have to be much larger than the thermal or concentration boundary layer. Surface vorticities predicted by the Galerkin method are quite reasonable. On the other hand, Figure 6 indicates that the surface pressure distribution is considerably higher than the values found by using the finite-difference method. It is interesting to note that total drag coefficients obtained through integration of surface vorticity and pressure distributions indicate a maximum error of 16% over the range $20 \leq N_{Re} \leq 500$. This points out the need for comparing local as well as integrated values when evaluating any approximate method. The results of the above comparison of the two methods of solution (finite-difference with Galerkin) are to be expected in this case, since over the front part of the sphere rapid changes occur with radius, whereas over the rear, angular variations are more important and eight terms involving the radial coordinate and only two terms involving angle are used. Including more angular terms in the trial stream function should alleviate these difficulties.

FINITE RADIAL MASS EFFLUX†

Boundary Conditions

At present there is no solution available that accurately predicts local Nusselt numbers in the wake region. Therefore, an idealized distribution over the entire sphere surface has been chosen that is similar at least in shape to experimental data. In practice such a distribution could certainly be more easily approximated by some sort of mechanical blowing. The distribution of radial velocities chosen is given by Equation (18).

$$(V_r)_{r=1} = \phi(1 + K\cos\theta) \tag{18}$$

where $(V_r)_{r=1}$ is the dimensionless radial velocity at the surface and ϕ and K are positive constants. This particular distribution gives a maximum and a zero flux at the frontal and rear stagnation points, respectively. This distribution resembles one that might be obtained for a sphere in a forced convection field. The limiting case of a constant flux independent of angle ($K = 0$) might be found in a strong radiation field.

The stream function for such a flow field takes the form:

$$\Psi = \phi(\cos\theta - 1) + \frac{\phi K}{4r}(\cos 2\theta - 1) \tag{19}$$

Equation (19) satisfies the potential flow equation:

$$E^2\Psi = 0 \tag{20}$$

The boundary conditions are:

Along the axis of symmetry

$$\theta = 0^\circ \quad \Psi = 0, \quad \zeta = 0 \tag{21}$$
$$\theta = 180^\circ \quad \Psi = -2\phi \quad \zeta = 0$$

On the sphere surface

$$r = 1 \qquad \Psi = \phi(\cos\theta - 1) + (\phi K/4)(\cos 2\theta - 1)$$
$$\zeta = E^2\Psi/\sin\theta \tag{22}$$

Far from the sphere surface

$$\Psi = 1/2\, r^2 \sin^2\theta + \phi(\cos\theta - 1) + (\phi K/4r)(\cos 2\theta - 1) \tag{23}$$

It is noted that for the case of constant mass efflux ($K = 0$), Equation (19) satisfies the required conditions that $(V_\theta)_{r=1} = 0$ and $(V_r)_{r=1} = \phi$. The fact that $(V_\theta)_{r=1} = (\phi K/2)\sin\theta$ for $K \neq 0$ is not too disturbing since in all practical cases $(\phi K/2) << 1$.

METHODS OF SOLUTION

Analytical Method

Using the superposition principle, we can obtain a solution to Equation (4) that satisfies the necessary boundary conditions:

$$\Psi = \left(\frac{1}{2}r^2 + \frac{1}{4r} - \frac{3r}{4}\right)\sin^2\theta + \phi(\cos\theta - 1) + \frac{\phi K}{4r}(\cos 2\theta - 1) \tag{24}$$

Finite-Difference Method

The same methods have been used here as those used for the case of zero mass efflux. At $N_{Re} = 1$, values of $\phi = 0.1$, 1, 2, 5, and 10 with $K = 0$ were investigated to compare the analytic solution with the finite-difference method. Solutions for Reynolds numbers of 40 and 100 were also investigated. In these instances both constant and variable surface fluxes were used with $\phi = 0.1$ and $K = 1.0$.

Error-Distribution Method (Galerkin Method)

The trial stream function was obtained by superposition of Kawaguti's function and the radial flux term, namely

$$\Psi = \left(\frac{1}{2}r^2 + \frac{A_1}{r} + \frac{A_2}{r^2} + \frac{A_3}{r^3} + \frac{A_4}{r^4}\right)\sin^2\theta + \left(\frac{B_1}{r} + \frac{B_2}{r^2} + \frac{B_3}{r^3} + \frac{B_4}{r^4}\right)\sin^2\theta\cos\theta + \phi(\cos\theta - 1) \tag{25}$$

The constants were determined by using the same orthogonality relationships as those used by Kawaguti. Solutions were obtained for the entire laminar flow regime for various magnitudes of ϕ.

DISCUSSION OF RESULTS

The results reported here are for three cases: constant mass efflux over the sphere ($\phi = 0.1$, $K = 0$); variable flux, which results in the same volume transfer rates as in the first case ($\phi = 0.1$, $K = 1$); and constant mass efflux at one low Reynolds number ($\phi = 0.1$ to 10).

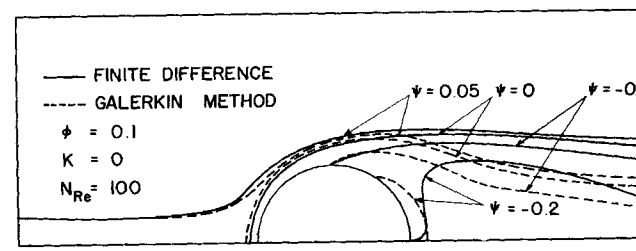

Fig. 7. Streamlines predicted by Galerkin and finite-difference methods (finite mass efflux).

†Derivation of equations for surface pressure and vorticity distributions, and friction and pressure drag coefficients for systems with variable mass efflux have been deposited as document 9160 with the American Documentation Institute, Photoduplication Service, Library of Congress, Washington 25, D. C., and may be obtained for $1.25 for photoprints or 35-mm. microfilm.

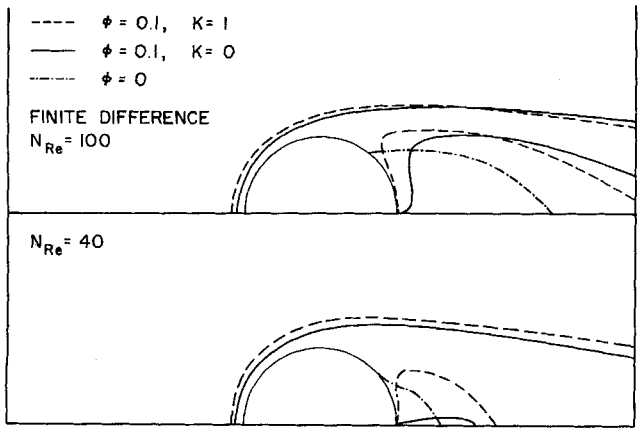

Fig. 8. Stagnation streamlines showing the effect of variable and constant mass efflux.

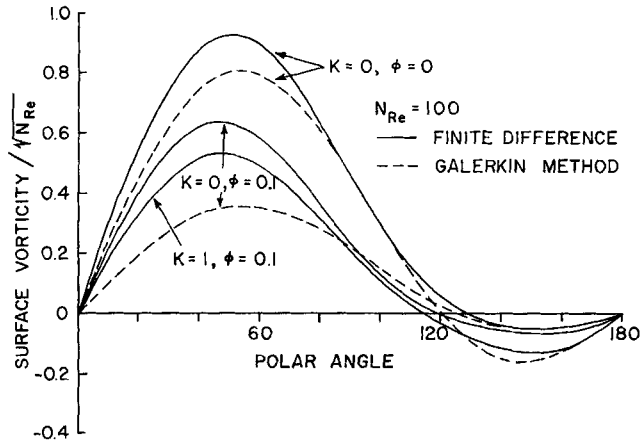

Fig. 9. Surface vorticity distributions showing the effect of constant and variable mass efflux.

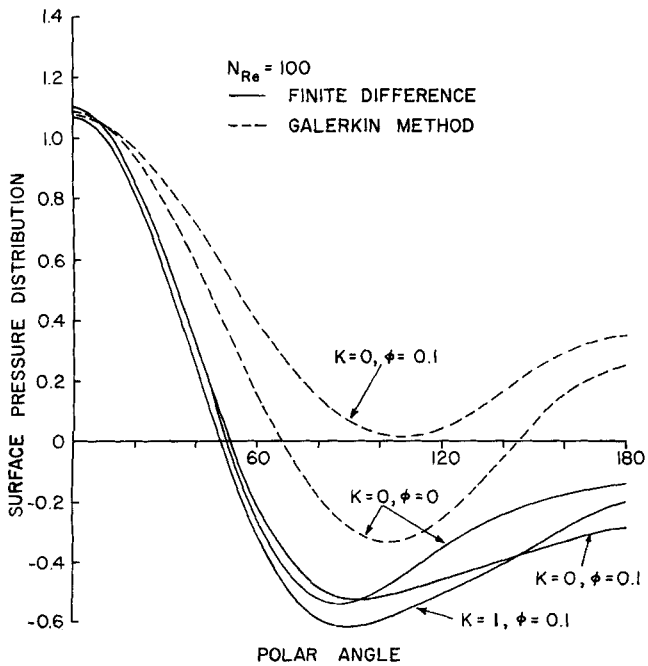

Fig. 10. Surface pressure distributions showing the effect of constant and variable mass efflux.

Table 3. Finite-Difference Results Showing the Effect of Radial Mass Efflux on Drag Coefficients

N_{Re}	ϕ	K	C_{DF}	C_{DP}	C_D
1.0	0.0	0.0	21.67	10.80	32.47
	0.1	0.0	21.37	10.79	32.16
	0.2	0.0	21.07	10.78	31.85
	0.5	0.0	20.19	10.75	30.94
	1.0	0.0	18.80	10.70	29.50
	2.0	0.0	16.29	10.62	26.91
	10.0	0.0	5.94	10.40	16.34
40	0.0	0.0	1.130	0.757	1.887
	0.1	0.0	0.818	0.830	1.648
	0.1	1.0	0.673	0.796	1.469
100	0.0	0.0	0.601	0.520	1.121
	0.1	0.0	0.332	0.621	0.953
	0.1	1.0	0.224	0.567	0.791

Figure 7 demonstrates again the ability of the Galerkin method to predict the flow behavior around the front of the sphere but indicates greater errors over the wake region. As before, this is related to the lack of sufficient angle terms in the trial stream function. The deviations illustrated in Figure 7 are the greatest observed up to $N_{Re} = 100$. The observed trends and poor agreement of the surface vorticity and pressure distribution, Figures 9 and 10, are similar to those reported previously for the zero flux case.

The effect of radial mass efflux on the flow around the sphere is shown for Reynolds numbers of 40 and 100 in Figure 8. The stagnation streamline has moved away from the sphere and its location is strongly dependent upon the magnitude of the flux rather than its distribution. Mass flow also extends the vortex and pushes it away from the sphere; in the case of variable flux, the vortex ring is not pushed away as much because the efflux rate is much less at the rear stagnation point. The location of the vortex indicates that periodic vortex shedding would be expected to occur at large efflux rates. This is not predicted here since the time-dependent terms have not been included in Equations (1), (2), and (3).

The effect of radial mass efflux on drag coefficient is shown in Table 3. Surprisingly, only when there is a variation of mass efflux over the sphere surface is the drag affected appreciably. This suggests that nonuniform blowing might be used to reduce the drag on submerged objects. We are not certain whether such techniques have been exploited. This reduction in drag arises primarily because the surface vorticity decreases with increasing efflux (see Figure 9) but the pressure distribution is relatively insensitive to this process. The analytical solution predicts a constant drag coefficient independent of level and distribution of mass efflux and this is commensurate with the results at $N_{Re} = 1$ which are tabulated in Table 3.

The ability of the analytical solution to predict the position of the stagnation streamline is shown in Figure 11. The agreement is certainly reasonable up to $\phi = 2$, which is well beyond the limits of mass transfer.

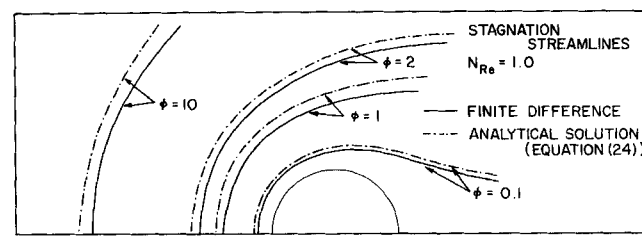

Fig. 11. Stagnation streamlines showing the effect of constant mass efflux at a low Reynolds number.

CONCLUSIONS

1. Accurate solutions of the Navier-Stokes equations for flow around a sphere for Reynolds numbers up to 100 are possible with the use of a finite-difference method and a digital computer (IBM 7040 and 7094).

2. Galerkin's error-distribution method as originally applied by Kawaguti allows reasonable description of the flow field up to the flow separation point.

3. Boundary-layer solution for surface vorticity up to the flow separation point is reasonably accurate for Reynolds numbers as low as 100.

4. Radial mass efflux affects the flow field around a sphere and reduces drag. This result is particularly apparent when the mass efflux is greatest at the frontal stagnation point.

Further investigations utilizing the finite-difference method to elucidate effects of acceleration, variable properties, and wall effect at high Reynolds numbers are underway. Other trial stream functions involving more angle terms and the variable flux for use with the Galerkin method are being formulated in the hope that a more satisfactory description of the flow field will be possible in this form so that a coupled solution with the energy equation may be attempted.

ACKNOWLEDGMENT

This study was supported in part by both the Pulp and Paper Research Institute of Canada and the National Research Council of Canada. L. L. Ross received scholarships from the National Research Council and the Shell Oil Company of Canada, Ltd. We appreciate the helpful suggestions of Vivien O'Brien.

NOTATION

A = lattice spacing in radial direction; sphere radius
A, B, C, D = constants in Equations (4*a*), (14), (15*a*), (15*b*), and (15*c*)
B = lattice spacing in angular direction
A_1-A_4, B_1-B_4 = constants in Equations (17) and (25)
C_{DP} = form or pressure drag coefficient
C_{DF} = friction drag coefficient
C_D = total drag coefficient
D = sphere diameter
d = diameter of Pitot tube
E^2 = differential operator
(I, J) = subscripts defining mesh point
F, G = functions of vorticity, Z, and θ
K = constant in Equation (18)
N = number of radial mesh points
N_{Re} = Reynolds number
n = iteration number
P = surface pressure distribution
r = radial spherical polar coordinate
R = position of outer, concentric, spherical boundary
U = mainstream velocity
V_θ = tangential velocity component
V_r = radial velocity component
W, WW = relaxation factors in Equations (9) and (10), respectively
Y_1, Y_2, Y_3 = dimensions of vortex ring
Z = modified radial spherical polar coordinate

Greek Letters

ζ = vorticity
θ = angular spherical polar coordinate
θ_s = flow separation angle as measured from rear stagnation point
Ψ = stream function
ν = kinematic viscosity
ϕ = constant in Equation (18)

LITERATURE CITED

1. *WADC Tech. Rept. 56-344 ASTIA Document No. Ad-118142* (Mar., 1957).
2. Torobin, L. B., and W. H. Gauvin, *Can. J. Chem. Eng.*, **37**, 129 (1959).
3. Castleman, R. A., *Natl. Advisory Committee Aeronaut. Tech. Note 231* (1926).
4. Eisner, F., *Proc. 3 Intern. Congr. Appl. Mech.*, Stockholm (1931).
5. Muttray, H., "Handbuch der Experimental Physik," Wien and Harms, Leipzig (1932).
6. Rouse, H., "Monogram for Settling Velocity of Spheres," Ann. Rept. Comm. Sed., Natl. Res. Council (1937).
7. Lapple, C. E., "Fluid and Particle Mechanics," Univ. Delaware, Newark (1954).
8. Schiller, L., and Z. Neuman, *Ver. Deut. Ing.*, **77**, 318 (1933).
9. Kljachko, L. S., *Heat Ventilation (U.S.S.R.)*, No. 4 (1934).
10. Langmuir, I., and K. Blodgett, *A.A.F. TR 5418* (1946).
11. Tomotika, S., and T. Aoi, *Quart. J. Mech. Appl. Math.*, **3**, 140 (1950).
12. Cooper, R. D., and M. P. Tulin, *AGARD No. 12* (1955).
13. Schiller, L., and W. Linke, *Natl. Advisory Committee Aeronaut. Tech. Note 715* (1933).
14. Nemenyi, P., *Trans. Am. Geophys. Union*, **21**, 633 (1940).
15. Williams, D. H., *Phil. Mag.*, **29**, 526 (1915).
16. Nisi, H., and A. W. Porter, *ibid.*, **46**, 754 (1923).
17. Taneda, S., *Rept. Res. Inst. Appl. Mech. (Japan)*, **4**, 99 (1956).
18. Oseen, C. W., *Ark. Mat. Astr. Rys.*, **6**, No. 29 (1910).
19. Goldstein, S., *Proc. Roy. Soc. (London)*, **123A**, 225 (1929).
20. Tomotika, S., and T. Aoi, *Quart. J. Mech. Appl. Math.*, **3**, 140 (1950).
21. Pearcy, T., and B. McHugh, *Phil. Mag.*, 7 Ser., 783 (1955).
22. Schlichting, Hermann, "Boundary Layer Theory," 4 ed., McGraw-Hill, New York (1955).
23. Acrivos, Andreas, *A.I.Ch.E. J.*, **6**, 410 (1960).
24. Eckert, E. R. G., *Natl. Advisory Committee Aeronaut Tech. Note 2733* (1952).
25. Spalding, D. B., *Appl. Mech. Rev.*, **15**, 505 (1962).
26. Millikan, C. B., *Trans. Am. Soc. Mech. Engrs.*, **54**, 29 (1932).
27. Tomotika, S., and I. Imai, *Rept. Aero. Res. Inst., Tokyo Imperial Univ. No. 167* (1938).
28. Tomotika, S., *Brit. Aeronaut. Res. Committee, Rank M, 1678* (1935).
29. ———, and I. Imai, *Proc. Phys. Math. Soc. Japan*, **20**, 288 (1938).
30. Flachsbart, O., *Phys. Z.*, **27**, translated, *Natl. Advisory Committee Aeronaut. Tech. Note 475* (1928).
31. Fage, A., *Brit. Aeronaut. Res. Committee, Rand M, 1766* (1936).
32. Frössling, N., *Gerlands Beitr. Geophys.*, **52**, 170 (1938).
33. Baird, M. H. I., and A. E. Hamielec, *Can. J. Chem. Eng.*, **40**, 119 (1962).
34. Hamielec, A. E., and A. I. Johnson, *ibid.*, 41.
35. Hamielec, A. E., S. H. Storey, and J. M. Whitehead, *ibid.*, **41**, 246 (1963).
36. Flumerfelt, R. W., and J. C. Slattery, *Chem. Eng. Sci.*, **20**, 157 (1965).
37. Hadamard, J. S., *Compt. Rend.*, **152**, 1735 (1911).
38. Jenson, V. G., *Proc. Roy. Soc. (London)*, **249A**, 346 (1959).
39. Kawaguti, M., *Rept. Sci. Res. (Tokyo)*, **2**, 66 (1948).
40. Stokes, G. G., *Trans. Cambridge Phil. Soc.*, **9**, 51 (1851).
41. Snyder, L. J., T. W. Spriggs, and W. E. Stewart, *A.I.Ch.E. J.*, **10**, 535 (1964).
42. Homann, F., *Natl. Advisory Committee Aeronaut. Tech. Note 1334* (1952).
43. Satapathy, R., and W. Smith, *J. Fluid Mech.*, **10**, 561 (1961).
44. Sherman, F. S., *Natl. Advisory Committee Aeronaut. Tech. Note 2995* (1953).

Manuscript received December 23, 1965; revision received July 14, 1966; paper accepted July 18, 1966.